JOURNAL OF CATALYSIS **164,** 70–81 (1996)
ARTICLE NO. 0364

Iron Oxide and Chromia Supported on Titania-Pillared Clay for Selective Catalytic Reduction of Nitric Oxide with Ammonia

Linda S. Cheng,* Ralph T. Yang,*,†,[1] and Ning Chen†

*Department of Chemical Engineering, State University of New York at Buffalo, Buffalo, New York 14260; †Department of Chemical Engineering, University of Michigan, Ann Arbor, Michigan 48109

Received March 18, 1996; revised July 29, 1996; accepted July 30, 1996

TiO_2-pillared clay (PILC) with high surface area, large pore volume, and large interlayer spacing was used as the support for mixed Fe_2O_3 and Cr_2O_3 as the catalyst for selective catalytic reduction (SCR) of NO with NH_3. The Fe/Cr ratio was varied at a fixed total amount of oxide dopant of 10% (wt). The Fe–Cr/TiO_2-PILC with Fe/Cr = 3 showed the highest activity. Compared with commercial V_2O_5/TiO_2 catalysts, the activity (on a per gram basis) of the doped pillared clay was approximately twice as high under H_2O- and SO_2-free conditions and was approximately 40% higher under conditions with H_2O and SO_2. In addition, its activity for SO_2 oxidation was only 20%–25% of that of the V_2O_5-based catalysts. TPD of NH_3 on the Fe–Cr/TiO_2-PILC catalyst showed that both M=O and M–OH (M=Fe or Cr) were necessary for the SCR reaction. *In situ* **IR spectra of NH_3 showed that there was a higher Brønsted acidity than the Lewis acidity on the surface under reaction conditions and that there existed a direct correlation between the SCR activity and the Brønsted acidity among pillared clays with different Fe/Cr ratios. These results, along with the transient response to O_2, indicated that a similar mechanism to that on the V_2O_5 catalyst was operative. The TiO_2-pillared clay used as the support also contributed to the high activity of the Fe–Cr catalyst. The TiO_2 pillars combined with the tetrahedral SiO_2 surfaces of the clay apparently gave rise to a high dispersion of Fe_2O_3.**

INTRODUCTION

Selective catalytic reduction (SCR) of nitrogen oxides with ammonia is of increasing commercial interest for stationary source applications. V_2O_5/TiO_2-based catalysts are presently used. A comprehensive review on the subject is available (1). The mechanism of the reaction on V_2O_5/TiO_2 is reasonably understood, although several different mechanisms have been proposed (1–5). Despite the high activities of the vanadia-based catalysts, major disadvantages remain and there are continuing efforts for developing new catalysts (1); pillared clays are particularly promising (6–10).

As a unique two-dimensional zeolite-like material, pillared interlayer clay (PILC) has attracted increasing interest for both its adsorption (11, 12) and catalytic properties. Pinnavaia (13), Burch (14), and Figueras (15), have given comprehensive reviews on the preparation, characterization, and applications of pillared clay as catalysts.

Because of its large pores, the early interest in PILC was in the possibility of replacing zeolite as the catalyst for fluid catalytic cracking. However, this possibility failed to realize due to excessive carbon deposition and limited hydrothermal stability of the pillared clay structure. These problems would not arise for the SCR reaction because the SCR conditions are far less severe than the FCC conditions. Besides FCC, PILCs have been studied for catalyzed alcohol dehydration, alkylation, and other acid catalyzed reactions. A pillared titanium phosphate was used as the support for V_2O_5 for the SCR reaction (14).

Both Lewis and Brønsted acid sites exist on pillared clays, with a larger proportion being Lewis acid sites. The acidity and acid site types (Brønsted or Lewis) depend on the exchanged cations, preparation method, and the starting clay.

Our discussion will begin with the Brønsted acidity because of its importance in selective catalytic reduction of NO by NH_3 (2, 7, 17). Two sources for Brønsted acidity have been discussed in the literature. One derives from the structural hydroxyl groups in the clay layer (18). The most likely proton site for some smectites (e.g., montmorillonite) is located at the Al(VI)–O–Mg linkage, where Al(VI) is the octahedrally coordinated Al, and Mg is one that has substituted an Al in the octahedral layer. For other clays, e.g., beidellite and saponite, the proton sites are located at the Si–O–AlOH groups resulting from isomorphous substitution of Si by Al in the tetrahedral layer. Another source of protons derives from the cationic oligomers which upon heating decompose into metal oxide pillars and liberate protons. It has been reported from many studies that both Lewis and Brønsted acidities decrease with temperature of calcination (15, 18). The disappearance of Brønsted acidity

[1] Address all correspondence to Ralph T. Yang at his present address at the University of Michigan. Current address for Linda S. Cheng is UOP, 50 E. Algonquin Rd., Des Plaines, IL 60017.

0021-9517/96 $18.00

is attributed to the migration of protons from the interlayer surfaces to the octahedral layer within the clay layer where they neutralize the negative charges at the substitution atoms (such as Mg). However, it is known that upon exposure to NH_3 the migration can be reversed so the proton is again on the surface to form ammonium ions. This is important to the SCR reaction.

A major advantage of pillared clays for SCR application (to replace the commercial V_2O_5/TiO_2) is its potential resistance to poisoning. The chemistry of poisoning of the Brønsted acid sites in the SCR reaction is reasonably understood (17). A significant contributor to catalyst poisoning is apparently the deposition of As_2O_3 and other vapor species (that exist in combustion systems) within the pore structure of the vanadia catalyst. This problem can be alleviated by a catalyst design suggested by Hegedus and coworkers (19), which consists of a bimodal pore size distribution in the V_2O_5/TiO_2–SiO_2 catalyst; one group of pores is of the order of microns (macropores) and the other group is of the order of angstroms (micropores). The poisonous vapor species in the combustion gas such as As_2O_3 deposit on the walls of the macropores due to their low diffusivities. Since the macropores serve as feeder pores to the micropores, they provide the function of filters of poisons. The pore structure of any catalyst made of pillared clays would be unavoidably bimodal. The commercially available clays such as montmorillonite are of particle sizes of microns or fractions of a micron. A pelletized (or washcoat) PILC catalyst will contain feeder (or poison filter) pores in the interparticle spaces, whereas the intraparticle micropores contain the active catalyst surface for the SCR reaction.

The literature on TiO_2-PILC is scanty compared to other pillared clays. Research on TiO_2-PILC was initiated by Sterte (20, 21), who first reported the synthesis of titanium pillared clay using $TiCl_4$ solution in hydrochloric acid. Yamanaka *et al.* (22) later prepared TiO_2-PILC with the hydrolysis of Ti isopropoxide as the intercalating agent. TiO_2-PILCs prepared from different Ti-alkoxides, particularly $Ti(OEt)_4$ were discussed by Del Castillo and Grange (23). Bernier *et al.* (24) studied the influence of temperature on TiO_2-pillared clay synthesis. Yang *et al.* (6) reported SCR activity on TiO_2-PILC, along with other pillared clay catalysts. SCR activity of TiO_2-PILC, particularly sulfated forms, was studied by Del Castillo *et al.* (10).

In this study, a substantial improvement on the SCR activity of TiO_2-PILC is achieved by adding dopants. The reason for choosing TiO_2-PILC is that TiO_2-PILC has the following desirable characteristics:

(a) high thermal and hydrothermal stability among all the pillared clays as demonstrated by TGA results (24);

(b) large pore sizes that allow further incorporation of active ingredients without hindering pore diffusion (21);

(c) Intercalating TiO_2 between the SiO_2 tetrahedral layers is a unique way of increasing surface area and acidity of the TiO_2 support;

(d) TiO_2 support interaction with the metal oxide dopants is another advantage resulting in higher catalytic activity;

(e) Titania-based SCR catalysts have been found to be highly resistant to SO_2 poisoning, and also possess durability (25).

The objective of this work is to extend the earlier work through optimization of TiO_2 pillared clay preparation condition and to investigate the relationship between the properties of TiO_2-PILC and their catalytic properties after the addition of Fe_2O_3 and Cr_2O_3 for the SCR reaction. The ratio of the mixed oxides was an important factor for its SCR activity.

EXPERIMENTAL

Catalyst Preparation

The starting clay for the preparation of TiO_2-PILC was purified montmorillonite, i.e., a purified-grade bentonite powder from Fisher Company, with particles less than or equal to 2 μm. The pillaring agent, a solution of partially hydrolyzed Ti-polycations, was prepared by first adding $TiCl_4$ into 1–2 *M* HCl solution. The mixture was then diluted by slow addition of distilled water with stirring to reach a final Ti concentration of 0.82 *M*. HCl in amounts corresponding to final concentrations in the range 0.11–0.60 *M* were used in the preparation.

The solution was aged for 12 h at room temperature prior to its use. A 4-g amount of bentonite was dispersed in 1.0 L of distilled water by prolonged stirring (5 h). The amount of pillaring agent required to obtain a Ti/clay ratio in the range 5–20 (mmol of Ti)/(g of clay) was then added to the rigorously stirred suspension. The resulting product was left in contact with the solution for 18 h and then separated by vacuum filtration and washed with distilled water repeatedly until the liquid phase was free of chloride ions (by the silver nitrate test). The final product was air dried at 120°C for 12 h and then calcined at 300°C for 12 h. The sample was then ground and sieved to 100–325 mesh. Subsequently the pillared clay was impregnated with Cr_2O_3 using $Cr(NO_3)_3$ solution, followed by impregnation of Fe_2O_3 using $Fe(NO_3)_3$ solution. The catalyst was then dried at 120°C for 12 h and calcined at 400°C in air for 12 h.

Characterization

a. N_2 adsorption at 77 K. A Quantasorb Surface Area Analyzer (Quantachrome Corporation) was used to measure N_2 adsorption isotherm at liquid N_2 temperature (77 K). BET surface areas were calculated from the isotherms.

b. X-ray diffraction. A Nicolet/Stoe transmission powder diffractometer with CuKα radiation was used to measure

the X-ray diffraction patterns of samples which were mounted with the clay crystals unoriented.

c. ICP-AES. The composition of the clay samples was determined by a Thermo Tarrel Ash 61 inductively coupled argon plasma atomic emission spectrometer (ICP-AES). Details on the ICP-AES analysis procedures can be found elsewhere (26).

Catalytic Activity Measurement

The test reactor consisted of a quartz tube containing a quartz frit support. A catalyst sample was placed on the frit and covered with a layer of glass wood. The heating element was a coiled Nichrome wire. The reactor temperature was controlled by an Omega CN-2010 programmable temperature controller.

The flue gas was simulated by blending gaseous reactants. Two sets of flow meters were used to control the flow rates of the reactants. High flow rates (i.e., N_2, NH_3 or NO/N_2) were controlled by rotameters, whereas the low flow rates (i.e., SO_2, O_2) were controlled by mass flow meters (FM 4575 Linde Division). The premixed gases (0.8% NO in N_2 and 0.8% NH_3 in N_2) were supplied by Linde Division. Water vapor was generated by passing nitrogen gas through a heated gas-wash bottle containing distilled water. The tubings of the system were wrapped with heating tape to prevent the deposition of ammonium sulfate. NO concentration was continually monitored by a chemiluminescent NO/NO_x analyzer (Thermo Electron Corporation, Model 10). To avoid errors caused by the oxidation of ammonia in the converter of the NO/NO_x analyzer, an ammonia trap containing phosphoric acid solution was installed before the sample inlet. The standard conditions for the activity measurements are given in Table 1. Product N_2 concentration was also analyzed with a gas chromatograph (Gow Mac Series 550) installed with a molecular sieve 5A column using He as the diluent gas. In addition, the reaction product was also analyzed with an on-line mass spectrometer (UTI-100C).

TABLE 1

Standard SCR Reaction Conditions

Gas	Concentration
NO	1,000 ppm
NH_3	1,000 ppm
O_2	2.0%
SO_2 (when used)	1,000 ppm
H_2O (when used)	8.0%
N_2	Balance
Volume hourly space velocity	60,000 h^{-1}
Flow rate	500 cm^3 (STP)/min
Catalyst amount	0.3 g
Temperature	473–698 K

Besides pillared clay catalyst samples. V_2O_5/TiO_2 and WO_3–V_2O_5/TiO_2 catalysts were also used for comparison. These catalysts were prepared by incipient wetness impregnation as described elsewhere (17). The WO_3–V_2O_5/TiO_2 catalyst had the same composition and surface area as a European commercial SCR catalyst as described by Tuenter *et al.* (27). In addition, a commercial vanadia-based catalyst obtained from a major supplier in the United States (designated as Company X, name withheld under secrecy agreement) was also used for comparison.

SO_3 Analysis

To measure the amount of SO_3 from SO_2 oxidation during the SCR reaction, a conventional wet analysis method was adopted. With the same reactor as the one used for measuring the catalyst SCR activity, the effluent was bubbled through a $BaCl_2$ solution, where all SO_3 was captured and precipitated as $BaSO_4$. The precipitate was collected on an ashless filter paper which was burned along with the precipitate in a crucible, so the amount of the precipitate was accurately measured.

TPD Analysis

TPD analysis was carried out with the same system as the one used for the activity test, except that the diluent gas was helium. Elution peaks were detected by a gas chromatograph equipped with a thermal conductivity detector. In each TPD experiment, a sample weighting 0.10 g was placed in the reactor and experiments were conducted in the following steps:

(a) Pretreatment: Different oxidation states of SCR catalysts have been shown to have a marked influence on the presence of surface oxygen or hydroxyl groups on the surface; hence, the effects of different oxidation pretreatments were investigated. The "NH_3-reduced" samples were obtained after NH_3 adsorption at 150°C and subsequent TPD up to 450°C. The reoxidized samples were those oxidized in O_2 at 250°C for 1.5 h.

(b) Adsorption: After the pretreatment, the catalyst was purged in He for an hour. The probe molecule, NH_3 or NO, was then adsorbed from a flowing gas stream at room temperature for 2 h. The mole fraction of NH_3 or NO was 3000 ppm in He. Helium was then used to purge the system, which usually took an hour.

(c) TPD: The temperature-programmed desorption was performed by ramping the temperature at 10°C/min from 25°C to 450°C. The desorbed molecules were detected by a gas chromatograph as well as a mass spectrometer, using He as the carrier gas. Water produced from dehydroxylation was desorbed simultaneously with NH_3. The NH_3 TPD spectrum was obtained by subtracting the water desorption spectrum obtained with the same catalyst which had not adsorbed NH_3.

FTIR Characterization

Infrared spectra were measured with a Nicolet Impact 400 FT-IR spectrometer. Self-supporting wafers of 1-cm diameter were prepared by pressing approximately 20-mg pillared clay samples. The *in situ* IR spectra of NH_3 adsorbed on the pillared clay were recorded by using an IR cell that allowed the sample to be treated at different temperatures and different gas atmospheres.

RESULTS AND DISCUSSION

Optimization of TiO_2-Pillared Clay as Catalyst Support

The preparation conditions of the TiO_2-PILC are listed in Table 2. The degree of hydrolysis and oligomerization of titanium cations in hydrochloride solution was affected by various factors, mainly Cl and Ti concentrations, as discussed by Nabivanets and Kudritskaya (28). As a result the characteristics of the final intercalated clays will be different. With a Ti^{4+} concentration of 0.82 *M*, the influence of the HCl concentration was studied. The concentration of the HCl solution was varied from 0.11 *M* to 0.60 *M*. The surface areas of the pillared clay samples are shown in Table 3. The surface area and pore volume were strongly influenced by the Ti/clay ratio, with 10 and 20 mmol/g yielding desirable results. At a fixed Ti/clay ratio, the surface area increased as the HCl concentration was decreased. However, the effect of HCl concentration on the micropore size distribution was just the opposite, which will be discussed later. Since the HCl concentration controlled directly the hydrolysis and polymerization of titanium (IV) in the hydrochloric solution, it also led to different polymeric species that determined the final pillared clay pore structure.

The chemical compositions of the montmorillonite clay and three TiO_2-PILC samples were measured with ICP-AES analysis and are shown in Table 3. The conditions for the synthesis of the last two samples were identical, except for the $TiCl_4$ concentration, which were 10 and 5 mmol Ti/g clay, respectively. From the data in Table 3, it is seen that during intercalation, the alkali and alkaline earth cations were replaced. The cation exchange capacity (CEC) of the montmorillonite clay was calculated from the chemical composition given in the Table. The CEC of the clay was 103 meq/100 g. The exchanges of the CEC by the intercalating species were 90%, 87%, and 80% for samples 13, 14, and 15, respectively, as a result of different degrees of cross-linking.

TABLE 2

Synthesis Conditions of TiO_2-Pillared Clays

Sample	[HCl], M	Ti mmol/g clay
TiO_2-PILC-11	0.11	20
TiO_2-PILC-12	0.60	20
TiO_2-PILC-13	0.11	10
TiO_2-PILC-14	0.60	10
TiO_2-PILC-15	0.60	5

TABLE 3

Chemical Compositions (in wt%) of Clay and TiO_2-Pillared Clays

Oxides	Bentonite	TiO_2-PILC-13	TiO_2-PILC-14	TiO_2-PILC-15
SiO_2	54.72	36.90	39.69	41.69
Al_2O_3	15.98	9.34	9.66	11.66
MgO	1.94	0.87	1.07	1.88
Fe_2O_3	2.93	1.47	1.73	2.20
TiO_2	0.12	37.48	35.16	29.18
Na_2O	2.04	0.14	0.22	0.24
CaO	0.82	0.03	0.03	0.16
K_2O	0.34	0.21	0.24	0.27

X-ray powder diffraction patterns of the montmorillonite and TiO_2-pillared clays are shown in Fig. 1. The d_{001} peak for the unpillared clay was at $2\theta = 7.8^\circ$. Upon intercalation the d_{001} peak shifted toward lower 2θ values, corresponding to increases in the d_{001} spacing. The d_{001} spacings of the pillared clays ranged from 29.4 to 28.0 Å. Subtracting 9.6 Å, the thickness of the clay layer (29), we obtained free spacing values ranging from 19.8 to 18.0 Å. Ti^{4+}-hydrolysis was discussed by Baes and Mesmer (30). A study by Einaga (31) on Ti^{4+}-hydrolysis and polymerization suggested the existence of a polymeric cationic species. $(TiO)_8(OH)_{12}^{4+}$. However, the structure of the complex is presently unknown. The interlayer spacing of the TiO_2-PILC was among the largest in all pillared clays. This was a desirable result as a catalyst support.

Table 4 shows the surface areas and pore volumes of the TiO_2-pillared clay samples. The values of surface area were calculated from the BET equation using N_2 adsorption (at 77 K). Samples 11, 13, and 14 showed high surface area above 300 m^2/g and N_2 pore volume at around 0.2 cm^3/g. The liquid nitrogen adsorption isotherms showed a typical type-II behavior, which indicated that both micropores and mesopores existed in the TiO_2-PILC. While the BET surface area increase was generated mostly through

TABLE 4

Surface Areas and Pore Volumes of TiO_2-Pillared Clays

PILC	BET S.A. m^2/g	Pore volume cm^3/g
TiO_2-PILC-11	343	0.20
TiO_2-PILC-12	201	0.18
TiO_2-PILC-13	402	0.24
TiO_2-PILC-14	308	0.21
TiO_2-PILC-15	171	0.14
Clay (Bentonite)	34	0.07

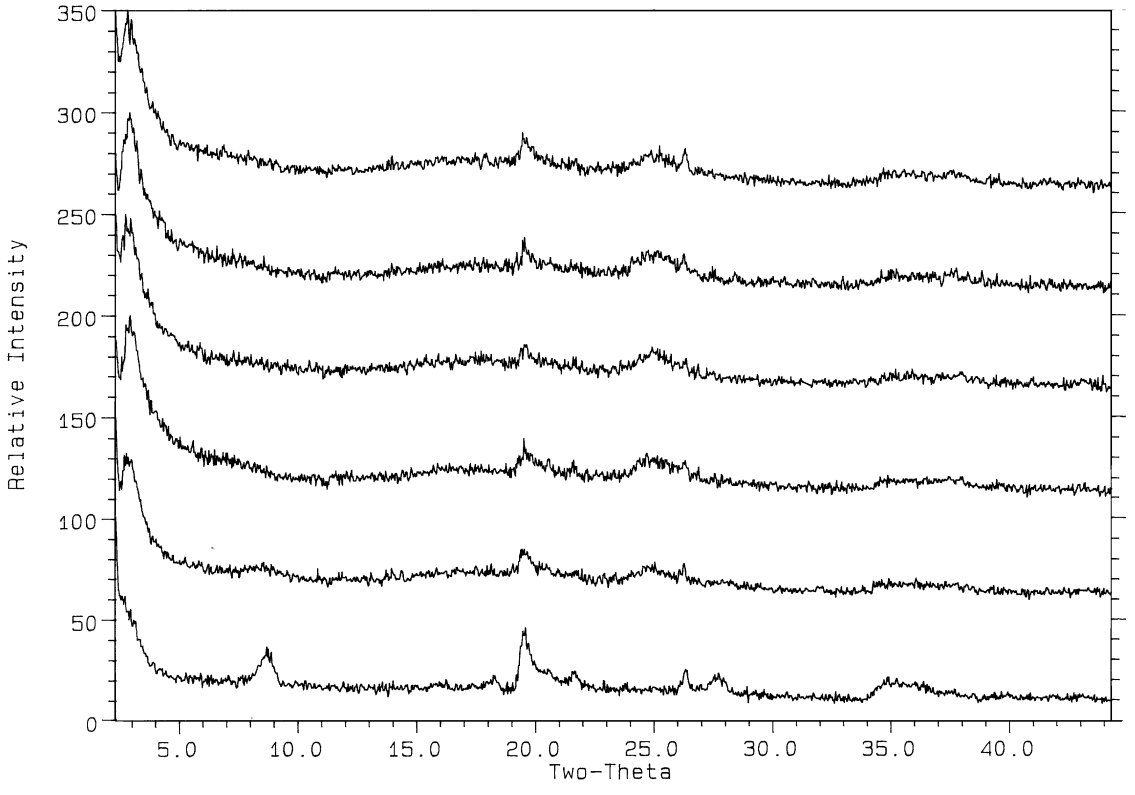

FIG. 1. X-ray powder patterns (CuKα source) for (from top down): TiO_2-PILC-11, TiO_2-PILC-13, TiO_2-PILC-14, TiO_2-PILC-12, TiO_2-PILC-15, and unpillared clay.

the micropore volume increase due to pillaring of the clay layers, contribution to the surface area increase from mesopores and macropores was also known to be significant, possibly due to the change in stacking of the clay platelets.

TiO_2-PILC-14 was used as the support for dopants due to its high surface area, pore volume, and large pores. Samples 11 and 13 were equally suitable, although not used.

Silica-titania mixed oxides have been proposed as the optimal support for the vanadia-based catalyst for NH_3 SCR of NO_x, due to the fact that through coprecipitation, the surface area of the support is markedly increased as compared to TiO_2 support alone (32). TiO_2-PILC is another unique way to prepare highly dispersed TiO_2 on SiO_2 since as pillars. TiO_2 is in direct contact with the silica layers of the clay, and the TiO_2-pillared clays possess high surface area, pore volume, and pore size.

SCR Catalytic Activity

Along with V_2O_5, iron and chromium oxides are the most active NH_3 SCR catalysts (1). Nobe and Bauerle (33) and Markvart and Pour (34) reported high SCR activities of Fe–Cr oxides supported on alumina. Nobe and coworkers later reported high SCR activities on a variety of Fe–Cr–V oxide mixtures supported on Al_2O_3 and TiO_2 (35, 36). In particular, a ratio of Fe/Cr = 9 yielded the highest activity (35). Amorphous chromia (36–39) and Cr–Fe–Al aerogels (40) also exhibited high SCR activities. For these reasons, Fe–Cr oxides were chosen for this study.

The SCR activity can be represented by a first-order rate constant (k), since the reaction is known to be first order with respect to NO and zero-order in NH_3 (under stoichiometric conditions) on a variety of metal oxides (1, 17, 41, 42). By assuming plug flow reactor (in a fixed bed of catalyst) and free of diffusion limitation, the rate constant can be calculated from the NO conversion (X) by

$$k = -\frac{F_0}{[NO]_0 W} \ln(1 - X), \qquad [1]$$

where F_0 is the molar NO feed rate, $[NO]_0$ is the molar NO concentration at the inlet (at the reaction temperature), and W is the catalyst amount. The catalyst amount was expressed in grams rather than in surface area or active sites, since the true surface area and active sites were not known.

Steady-state NO conversion data were obtained for catalysts doped with various ratios of Fe_2O_3/Cr_2O_3 and at various temperatures. The conversion-temperature data for the most active catalyst are shown in Fig. 2. From these data, the first-order rate constants were calculated. The rate constants are compared in Table 5. The total amount of Fe–Cr oxides was fixed at 10% (wt) of the pillared clay, while the

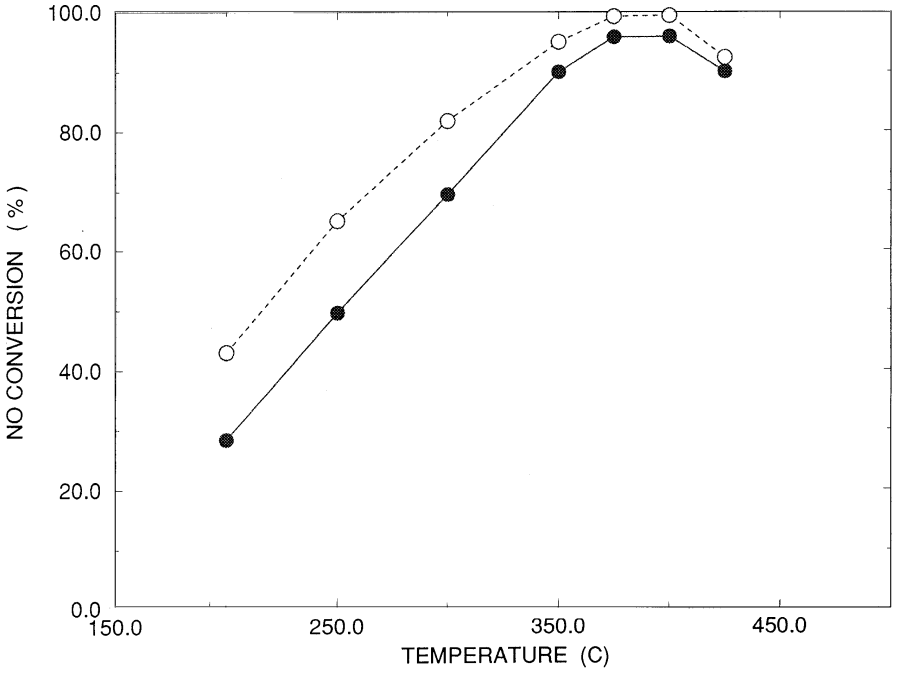

FIG. 2. NO conversion on 7.5% Fe_2O_3 + 2.5% Cr_2O_3/TiO_2-pillared clay. Reaction conditions: NO = NH_3 = 1000 ppm, O_2 = 2%, H_2O = 8%, SO_2 = 1000 ppm, N_2 = balance, GHSV = 60,000 h^{-1}, without SO_2 and H_2O (○), with SO_2 and H_2O (●).

Fe/Cr ratio was varied. Figure 2 shows the typical temperature window, with a peak in the range 375°–400°C. The rate constants for the vanadia-based catalysts (a commercial catalyst and a catalyst with $V_2O_5 + WO_3$ that was similar to a commercial catalyst) were also measured and included in the comparison.

The first conclusion drawn from the results was that the Fe–Cr/TiO_2-PILC with an Fe/Cr = 3 was the most active catalyst. More importantly, the doped catalysts were substantially more active than the commercial vanadia-based catalysts. The Fe–Cr/TiO_2-PILC catalyst was 30%–50% more active than the vanadia catalysts under conditions with SO_2 and H_2O.

The presence of SO_2 alone only slightly increased the activity of the Fe–Cr catalyst. This was similar to the vanadia catalyst, due to an increase of the acidity on the catalyst (17).

The effect of water on the Fe–Cr/TiO_2-PILC was also similar to that on the vanadia catalyst. Water substantially reduced the SCR activity. The SCR activity was totally reversible; i.e., the steady-state NO conversion was recovered by switching off the water vapor. This result was also similar to vanadia. The effect of water on NH_3 SCR has been discussed on vanadia catalyst (17, 43) and on other oxides including Cr_2O_3 (38) and was reviewed in (38).

Previous studies showed that no significant amounts of N_2O were formed on Fe_2O_3 catalyst. However, N_2O was formed (along with N_2) on Cr_2O_3 catalysts (38–40), depending on the crystallility (38). Crystalline α-Cr_2O_3 gave rise to N_2O while amorphous form did not (38). Formation of N_2O was proposed as the product of oxidation of adsorbed NH_3 at temperatures higher than 100°C (39). Our results, Fig. 2, showed that the NO conversion reached over 96% in the temperature range 350°–400°C. Thus NH_3 was almost completely consumed (since 1000 ppm each of NH_3 and NO were used) by NO. This result was different from that of Wong and Nobe (36, 44) on Fe–Cr/TiO_2 or Al_2O_3. Their Fe_2O_3–Cr_2O_3 catalyst showed maximum NO conversion at

TABLE 5

First-Order Rate Constants of TiO_2-PILC Catalysts with Doped Fe_2O_3 and Cr_2O_3

Catalyst sample	First-order rate constant (k), $cm^3/g/s$		
	no SO_2, no H_2O	with SO_2	with SO_2 and H_2O
TiO_2-PILC (= A)	14	14	8
10% Fe_2O_3 (on A)	181	194	89
7.5% Fe_2O_3 + 2.5% Cr_2O_3 (on A)	305	309	192
5.0% Fe_2O_3 + 5.0% Cr_2O_3 (on A)	233	236	178
2.5% Fe_2O_3 + 7.5% Cr_2O_3 (on A)	152	152	87
10% Cr_2O_3 (on A)	140	140	104
Commercial V_2O_5 Catalyst (Company X)	158	—	129
$V_2O_5 + WO_3/TiO_2$ (4% V_2O_5 + 8% WO_3)	141	—	141

Note. NO = NH_3 = SO_2 = 1000 ppm, O_2 = 2%, H_2O = 8%, T = 375°C.

temperatures below 270°C, where NO conversion sharply declined as temperature was further increased due to NH_3 oxidation to form N_2O at higher temperatures. The reaction product analysis was performed in a separate experiment in which He was used as the carrier gas. The sample with 7.5% Fe_2O_3 and 2.5% Cr_2O_3 was used. The reaction temperature was 375°C and the conditions in Table 1 were followed. The on-line mass spectrometry results showed no detectable signals at m/e = 44 and 46, indicating that the concentrations of N_2O and NO_2 in the products were well below 1%. This result was consistent with that reported in the literature on other Fe–Cr catalysts. The lack of N_2O in the product was likely a result of the noncrystalline form of the Cr_2O_3 that was dispersed on the pillared clay.

The first-order rate constant given in Table 5 should be considered as an apparent rate constant, since diffusion limitation was clearly significant (7, 44). The rate constant was expressed on a per gram basis. It would have been desirable to express the rate constant on the basis of per surface area or active site. This was not done as explained as follows. The surface areas of the V_2O_5-based catalysts were approximately 30 m^2/g, and monolayer coverage could be assumed. The surface areas of the PILC were approximately 300 m^2/g; however, the surface area of the Fe_2O_3/Cr_2O_3 dopant was not known. The active sites on V_2O_5 are most likely dual sites of neighboring V=O and V–OH. The density of such dual sites has not been determined on any catalysts. On the Fe/Cr-PILC catalyst, we are also proposing that the active sites are the dual sites of Fe=O and Fe–OH (see the ensuing discussion). The density of such dual sites is also unknown. Since the surface area of the pillared clay is substantially higher than that of TiO_2 (which is used as the support for V_2O_5), it is entirely possible that vanadia is more active than the Fe/Cr catalyst on a per active site basis.

SO_2 Oxidation Activity

Oxidation of SO_2 to SO_3 is highly undesirable for the SCR reaction due to the formation of ammonium sulfate and environmental reasons (45). Vanadia-based catalysts have a high SO_2 oxidation activity (35), which has been a major concern in SCR operations. Effort has been made to either add certain oxides (such as WO_3) to the V_2O_5 catalyst or to use non-V_2O_5 catalysts for the purpose of decreasing SO_2 oxidation activity while maintaining high NO_x reduction activity (27, 45).

Using the wet chemical method described in the foregoing to quantitatively measure the amounts of SO_3 generated in the reaction effluents, SO_2 conversion for three catalysts were obtained. The activities for SO_2 oxidation were in the following order:

$$V_2O_5/TiO_2 > WO_3 + V_2O_5/TiO_2 > Fe_2O_3 + Cr_2O_3/TiO_2 - PILC. \quad [2]$$

The conversions for SO_2 to SO_3 were 2.6%, 2.0%, and 0.5%, respectively, for the three catalysts at 375°C. The Fe_2O_3–Cr_2O_3/TiO_2-PILC yielded much lower SO_3 than the V_2O_5-based catalysts. Results by Clark *et al.* (46), in their study of alumina-supported iron oxide and vanadium oxide catalysts, also showed that Fe_2O_3 was less active in SO_2 oxidation than V_2O_5. The low SO_2 oxidation activity is another advantage for the Fe–Cr/TiO_2-PILC catalyst.

Transient Response to O_2

Previous studies of various metal oxide SCR catalysts (34, 46) have shown the importance of oxygen in the reaction. Transient behavior of the catalyst was tested by turning off and on the oxygen in the gas phase. The NO conversion is shown in Fig. 3. The NO conversion declined steadily after O_2 was turned off. The first steady decline was relatively fast, lasting about 30 min. This was followed by a slower (but steady) decline. Switching O_2 back on resulted in an immediate increase in NO conversion, and the original conversion was restored quickly. Similar transient behavior has been observed for V_2O_5, Fe_2O_3, and Cr_2O_3 based catalysts (25, 36, 41, 46), indicating that the lattice oxygen was

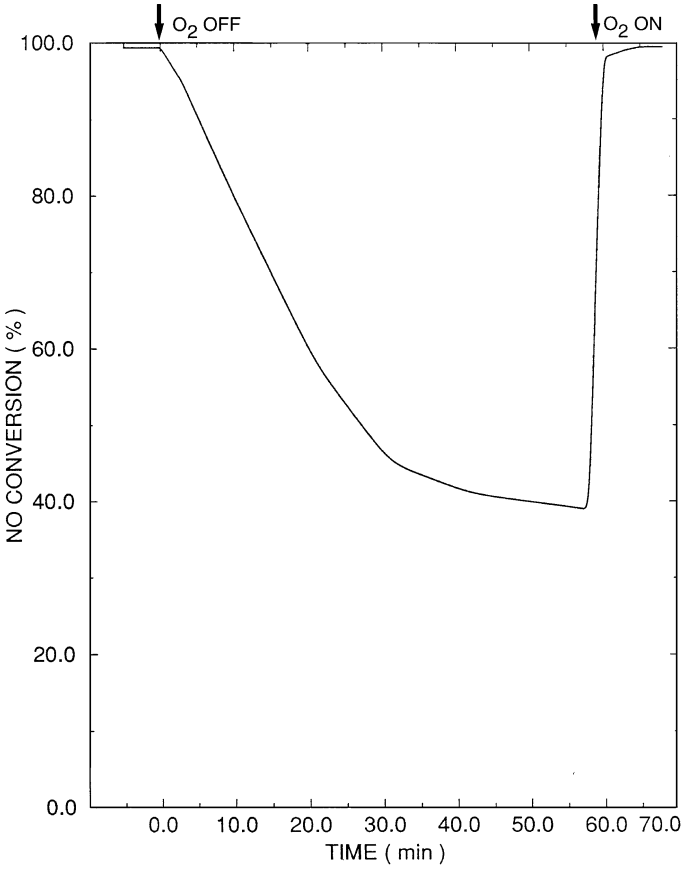

FIG. 3. Transient response on Fe–Cr/TiO_2-pillared clay upon switching off and on O_2. $T = 375$°C. The reaction conditions are with H_2O and SO_2; other conditions are shown in Table 1.

participating in the NO reduction reaction when O_2 was shut off.

From the data shown in Fig. 3, a quantitative estimate can be made on the amount of oxygen that was stored in the Fe_2O_3–Cr_2O_3 catalyst in comparison with that required for the SCR reaction (based on the known stoichiometry $6NO + 6NH_3 + 4O_2$). The NO conversion declined steadily from approximately 99% to 40% in 30 min. During this period of time, 0.29 mmol O_2 was required for the reaction. The total amount of oxygen stored in the supported $Fe_2O_3 + Cr_2O_3$ was 0.28 mmol. This seemed to be a good agreement; however, it was not expected that all of the oxygen in the oxides would be available for the reaction. This could be explained in view of the second decay in NO conversion, after $t = 30$ min. The second decay indicated two possibilities. One was a reaction in which the oxygen was supplied by the TiO_2, through the $Fe_2O_3 + Cr_2O_3$ layer. The other was the SCR reaction without O_2 (1). In view of the second decay, it was reasonable to assume that, during the first decay, only the portion of the reaction above 40% NO conversion was due to the oxygen stored in the $Fe_2O_3 + Cr_2O_3$. This portion of the reaction required only 0.13 mmol oxygen from the lattice oxygen. The role of O_2 in the SCR reaction on V_2O_5 is well understood (2, 47, and the earlier work by Murakami and coworkers referenced in 47). The similar and reversible transient behaviors of the Fe–Cr catalyst also pointed to a similar reaction mechanism.

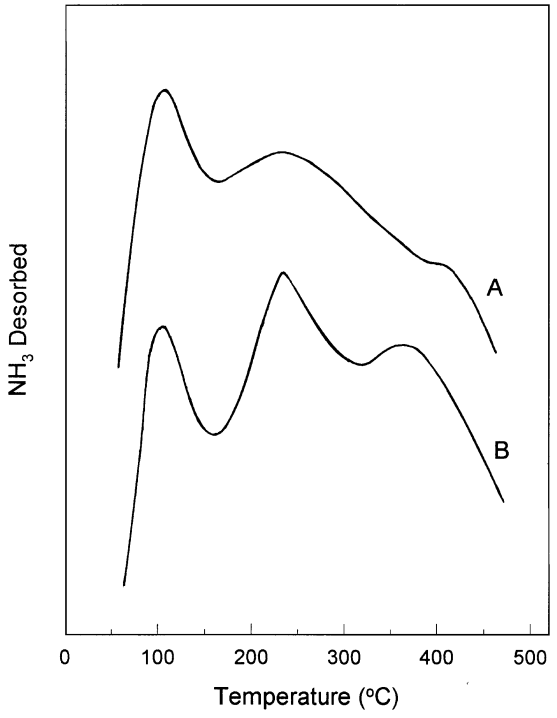

FIG. 4. TPD of NH_3 on (A) undoped TiO_2-pillared clay and (B) that doped with 7.5% $Fe_2O_3 + 2.5\%$ Cr_2O_3. Adsorption of NH_3 was at 3000 ppm at r.t. followed by heating at 10°C/min in He.

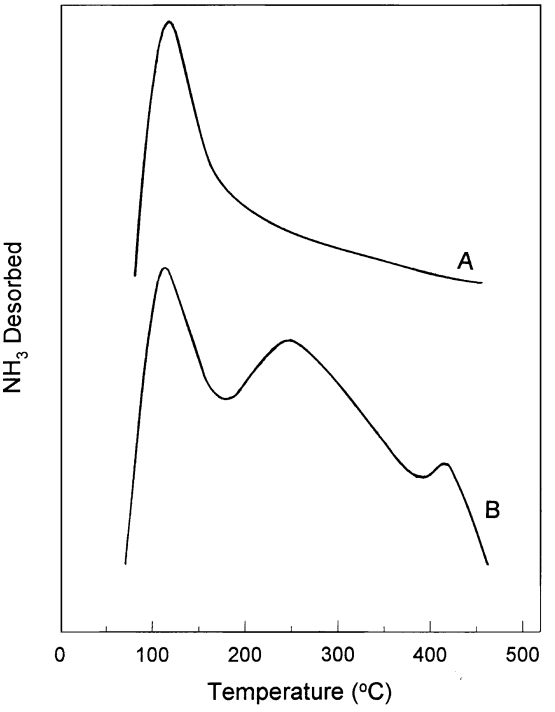

FIG. 5. TPD of NH_3 on (A) NH_3-reduced and (B) reoxidized Fe–Cr/TiO_2-pillared clay (NH_3 reduction was at 150°C, and reoxidation was at 250°C).

TPD of NH_3 and NO

TPD spectra of NH_3 on TiO_2-pillared clay and on that doped with Fe–Cr (7.5% $Fe_2O_3 + 2.5\%$ Cr_2O_3/TiO_2-PILC) are shown in Fig. 4. Three distinctive desorption peaks were seen, with maxima at approximately 105°C, 240°C, and 370°–410°C. For convenience in discussion, these three peaks were designated α, β, and γ adsorbed states. It is clearly seen that the Fe–Cr doped pillared clay chemisorbed substantially larger amounts of the strongly bonded NH_3, i.e., β and γ states, whereas the amounts of the weakly bonded α state were approximately the same on the two catalysts. Also, the peak temperatures of the strongly adsorbed γ state were different. The γ state desorbed at a higher temperature on the undoped pillared clay, indicating a higher desorption activation energy.

TPD spectra of NH_3 on reduced and reoxidized Fe–Cr/TiO_2-PILC samples are shown in Fig. 5. As discussed in the foregoing section, the reduction was done by reacting with NH_3 at 150°C followed by desorption in He at a heating rate of 10°C/min up to 450°C. The "reduced" sample was subsequently cooled to 25°C for NH_3 adsorption and TPD measurement. For the "reoxidized" sample, the NH_3 "reduced" sample was oxidized in O_2 at 250°C for 1.5 h, followed by cooling to 25°C. The TPD spectrum of the reduced sample showed only the α peak. The TPD spectrum of the reoxidized sample showed partial restoration of the β

and γ species. However, the amounts of the β and γ species were substantially less on the reoxidized sample (Fig. 5B) as compared to that on the original sample (Fig. 4B). Along the lines of the results of previous TPD sutdies on SCR catalysts (37, 38, 48, 49) NH_3 reduction of the Fe–Cr/TiO_2-PILC surface would reduce the M=O and M–OH surface groups (where M denotes Fe or Cr) to from surface vacancies, as indicated by

$$Fe{=}O \xrightarrow{NH_3} Fe\square; \quad Fe{-}OH \xrightarrow{NH_3} Fe\square \qquad [3]$$

$$Cr{=}O \xrightarrow{NH_3} Cr\square; \quad Cr{-}OH \xrightarrow{NH_3} Cr\square. \qquad [4]$$

Upon reoxidation, the surface vacancies will be filled with oxygen to generate Fe=O and Cr=O surface species.

The difference between the fresh Fe–Cr/TiO_2-PILC sample and the reoxidized (after being, first, NH_3-reduced) sample was that the fresh sample had both M=O and M–OH surface species, whereas the reoxidized sample had only (or predominantly) M=O species. Comparing the TPD spectra on these two samples (Figs. 4B and 5B), it becomes clear that the extra amounts of the strongly chemisorbed β and γ species on the fresh sample were due to the M–OH groups, i.e., the Brønsted acid sites. The nature of the weak α state can also be understood by comparing all four TPD spectra in Figs. 4 and 5. The peak intensities and positions of the α species belong to physically adsorbed NH_3, irrespective of the chemistry of the sites.

The TPD results can be discussed with the results from the preceding section, i.e., the transient O_2 behavior. The SCR activity of the catalyst was reduced dramatically when O_2 was stopped; that is, the NH_3-reduced surface had little activity. It can be concluded that the α species was not related to the SCR reaction, whereas the β and γ species of NH_3 were involved in the SCR reaction. In the O_2 transient experiment, the SCR activity was fully restored after O_2 of the "reoxidized" sample in the TPD experiment. The catalyst in the SCR reaction was exposed to H_2O, since it was a reaction product, which formed M–OH groups on the surface. This point was clearly shown in our earlier work on V_2O_5/TiO_2 (17). The "reoxidized" sample in the TPD experiment, on the other hand, could not form M–OH groups and had only M=O groups.

From the discussion above, one may conclude that both M=O and M–OH groups (where M=Fe or Cr) on the Fe–Cr/TiO_2-PILC catalyst were responsible for the high SCR activity. This conclusion also points to the same mechanism for the SCR reaction on our catalyst as that on the V_2O_5/TiO_2 catalyst (2, 17, 47).

The TPD spectra of NO on fresh and NH_3-reduced Fe–Cr/TiO_2-PILC samples are shown in Fig. 6. The adsorption was at room temperature with 3000 ppm NO in He. Only a small amount of NO was adsorbed on the fresh catalyst (i.e., the active catalyst), with a desorption peak at

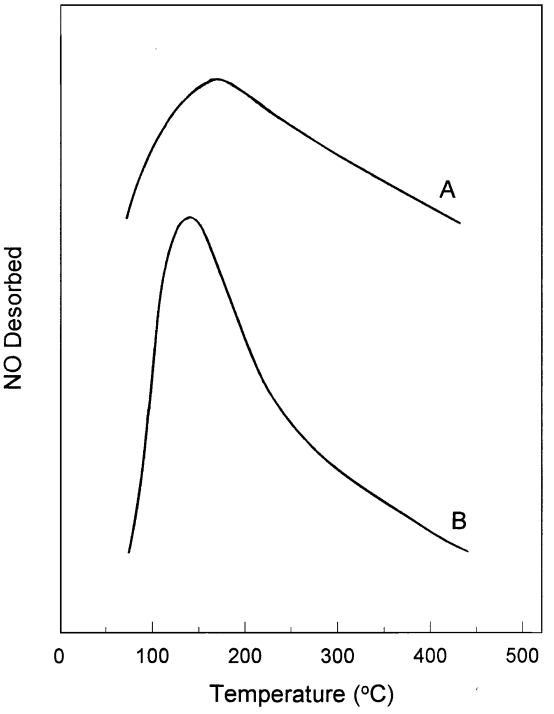

FIG. 6. TPD of NO on (A) fresh and (B) NH_3-reduced Fe–Cr/TiO_2-pillared clay. NO adsorbed at 3000 ppm at r.t. followed by heating at 10°C/min.

140°C. The amount of NO adsorbed on the NH_3-reduced surface was significantly higher, with a desorption peak at 150°C. The NO TPD spectra were similar to those on V_2O_5 (50, where NH_3 TPD was also shown to be similar to our catalyst), and on Fe_2O_3 (51). The metal ions on the reduced catalyst at a lower volume could more easily accommodate the antibonding electron of the NO molecule, hence the higher amount adsorbed. However, like vanadia, NO did not adsorb at temperatures where the catalyst had the highest SCR activity, i.e., 375°–400°C. This result also supports the conclusion that a similar reaction mechanism operates on both vanadia and the Fe–Cr/TiO_2-PILC catalysts.

The NH_3 TPD products were also subjected to on-line mass spectrometry analysis. At temperatures below 350°C, NH_3 was the predominant species. On the reoxidized sample, the amounts of N_2 and N_2O became significant at 350°C and increased steeply with temperature. At 400°C, the gaseous product contained approximately 20% N_2 and 5% N_2O, the balance being NH_3. A small signal at m/e = 48 was also observed but not identified.

Infrared Spectroscopy Study

Ammonia was used as a probe to investigate the nature and strength of the acid sites on the catalysts. Such information was obtained by studying the FTIR spectra of the adsorbed NH_3. Six catalysts were used in this study: fresh Fe–Cr/TiO_2-pillared clay, and five pillared clay samples

doped with 10% (wt) $Fe_2O_3 + Cr_2O_3$ at different Fe/Cr ratios, as shown in Table 5. *In situ* IR spectra were taken with 1% NH_3 in He in the gas phase, and at temperatures from 25°C to 400°C. All spectra were ratioed against the background with 1% NH_3.

Figure 7 shows the spectra of NH_3 adsorbed on the five Fe–Cr-doped pillared clay samples, at 25°C. The band at approximately 1450 cm^{-1} was due to the asymmetric bending vibration of NH_4^+ that was chemisorbed on the Brønsted acid sites. The band at approximately 1620 cm^{-1} was due to the asymmetric bending mode of ammonia coordinated on the Lewis acid sites. For all samples, there were substantially more Brønsted acid sites than Lewis sites. The undoped pillared clay showed no Brønsted acidity, and was not included for further study. By comparing the spectra in Fig. 7, the catalyst doped with Fe/Cr = 3 had the largest amounts of both Brønsted and Lewis acid sites. This catalyst also showed the highest SCR activity (Table 5).

The IR spectra of the chemisorbed ammonia as a function of temperature for the Fe/Cr = 3 catalyst are shown in Fig. 8. Both Brønsted and Lewis acidity decreased with increasing temperature. This was the pattern also exhibited by all other doped catalysts; hence they are not included in Fig. 8.

The SCR activity was clearly correlated to the Brønsted acidity. The correlation between the first-order rate constant and the Brønsted acidity for the five doped pillared clay samples is shown in Fig. 9. The undoped pillared clay had little Brønsted acidity, hence a low activity, and it was not included.

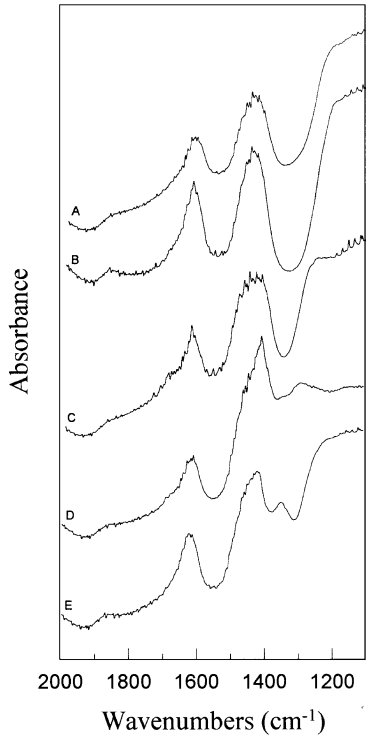

FIG. 7. FTIR spectra of chemisorbed NH_3 at 25°C on five TiO_2-pillared clays doped with: 10% Fe_2O_3 (A); 7.5% Fe_2O_3 + 2.5% Cr_2O_3 (B); 5% Fe_2O_3 + 5% Cr_2O_3 (C); 2.5% Fe_2O_3 + 7.5% Cr_2O_3 (D); 10% Cr_2O_3 (E).

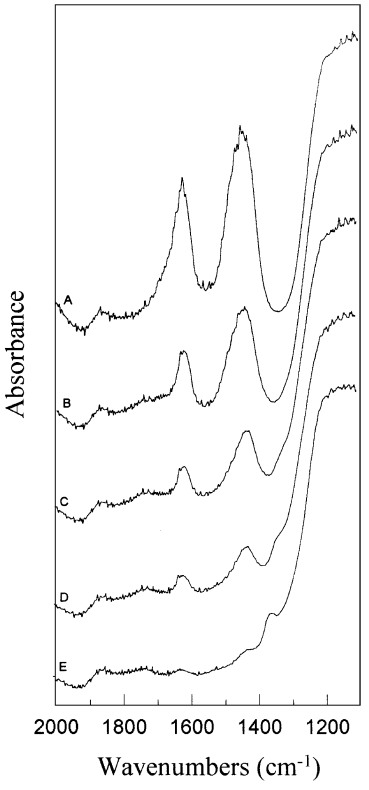

FIG. 8. FTIR spectra of chemisorbed NH_3 on 7.5% Fe_2O_3 + 2.5% Cr_2O_3/TiO_2-pillared clay at five temperatures: 25°C (A); 100°C (B); 200°C (C); 300°C (D); 400°C (E).

Reaction Mechanism and TiO_2-Pillared Clay Support

The undoped TiO_2-pillared clay showed little SCR activity, whereas that doped with Fe_2O_3 and Cr_2O_3 yielded high activities. The sample doped with 7.5% Fe_2O_3 and 2.5% Cr_2O_3, in particular, showed the highest activity.

TPD of NH_3 on the Fe–Cr/TiO_2-PILC catalyst (using both reduced and reoxided samples) showed that both M=O and M–OH (where M=Fe or Cr) were necessary for the SCR reaction. This result indicated that a similar mechanism was operative on this catalyst as that on V_2O_5/TiO_2 (2, 17, 47). The NH_3 TPD results also showed that a significant amount of NH_3 was chemisorbed on Fe–Cr/TiO_2-PILC in the temperature range where it had the highest activity (350°–400°C). On the contrary, TPD of NO showed that no or little NO could chemisorb at temperatures higher than 300°C. This result pointed to an Ely–Rideal type of mechanism; again, this was similar to the reaction on V_2O_5/TiO_2.

Using ammonia as the probe molecule, IR spectra showed that there was significantly more Brønsted acidity than Lewis acidity on the Fe–Cr/TiO_2-PILC. Also, a

significant amount of Brønsted acidity remained at temperatures as high as 400°C. By comparing the Brønsted acidities of Fe–Cr doped catalysts with different Fe/Cr ratios, it became clear that there was a direct correlation between the SCR activity and the Brønsted acidity. This correlation was also seen for the V_2O_5/TiO_2 catalyst (17). Moreover, the results of the O_2-transient experiment (i.e., SCR activity by turning off O_2 and readmitting O_2) on the catalyst yielded similar behavior as that on V_2O_5/TiO_2, indicating that M–OH was oxidized to M=O by O_2, and thus restored the activity. In addition, the similarity of the effects of SO_2 and H_2O on the Fe–Cr catalyst and V_2O_5/TiO_2 was also in line with a similar mechanism on both catalysts.

From the results and discussion given above, it is reasonable to suggest a similar mechanism for the reaction on the Fe–Cr/TiO_2-PILC catalyst at that on V_2O_5/TiO_2 (2, 17, 47). Such a mechanism is illustrated in Fig. 10.

Fe_2O_3–Cr_2O_3 mixtures on a variety of supports have been studied as the catalysts for the SCR reaction, as discussed in the foregoing. The unusually high activities observed on the TiO_2-pillared clay as a support indicates that unusual properties are available on this support. Based on the Mössbauer spectra of Fe_2O_3 doped on SiO_2–TiO_2, lizuka *et al.* (1982) (51) found that Fe_2O_3 was highly dispersed on SiO_2–TiO_2 and that the TiO_2 phase played a remarkable role for the dispersion of Fe_2O_3. Both faces of the montmorillonite clay layer are tetrahedral silica. The intercalation of TiO_2 pillars

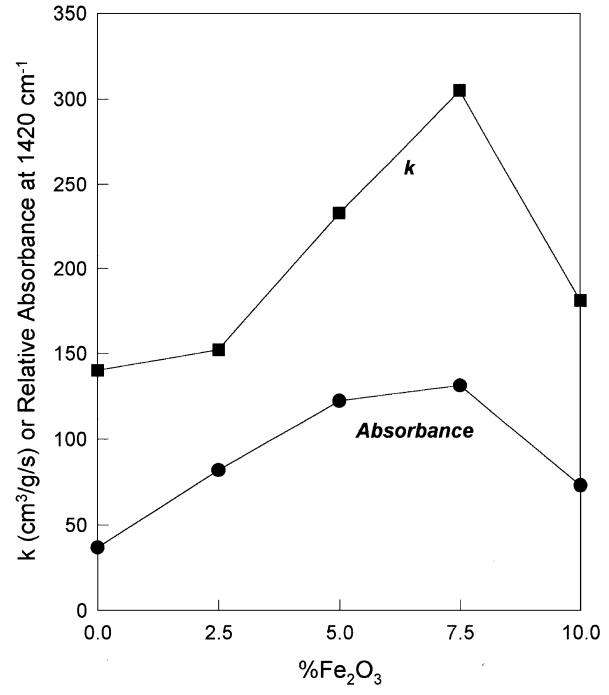

FIG. 9. SCR activity (expressed by first-order rate constant, k) at 375°C correlated with Brønsted acidity (expressed by relative absorbance of chemisorbed NH_3 at 300°C) for Fe–Cr/TiO_2-pillared clays, total $Fe_2O_3 + Cr_2O_3 = 10\%$.

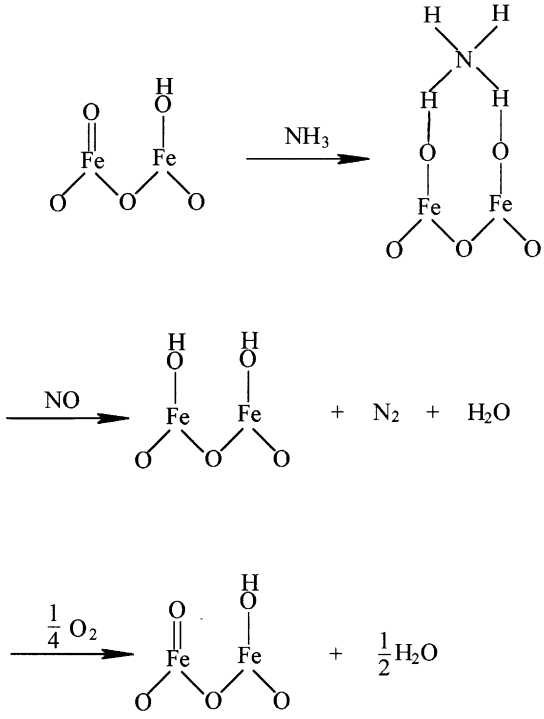

FIG. 10. Schematic of the mechanism of the SCR reaction on Fe–Cr/TiO_2 pillared clay, where Fe can be replaced by Cr.

of molecular dimensions between the clay layers provides a high surface area SiO_2–TiO_2 surface for the dispersion of Fe_2O_3 and Cr_2O_3. Therefore, the strong support effect of the TiO_2-pillared clay is to be expected. The combination of Fe_2O_3 (or Cr_2O_3) with TiO_2 is known to generate both Brønsted and Lewis acidities (52). The reason for the highest Brønsted acidity formed at an Fe/Cr ratio of 3 is not understood.

ACKNOWLEDGMENT

The work was supported by the Department of Energy, DE-FG22-93PC93217.

REFERENCES

1. Bosch, H., and Janssen, F., *Catal. Today* **2**, 369 (1988).
2. Topsøe, N. Y., Dumesic, J. A., and Topsøe, H., *J. Catal.* **151**, 241 (1995).
3. Went, G. T., Leu, L. J., Rosin, R. R., and Bell, A. T., *J. Catal.* **134**, 492 (1992).
4. Ozkan, U. S., Cai, Y., and Kumthekar, M. W., *J. Catal.* **149**, 390 (1994).
5. Odriozola, J. A., Heinemann, H., Somorjai, G. A., Garcia de la Banda, J. F., and Pereira, P., *J. Catal.* **119**, 71 (1989).
6. Yang, R. T., Chen, J. P., Kikkinides, E. S., Cheng, L. S., and Cichanowicz, J. E., *Ind. Eng. Chem. Res.* **31**, 1445 (1992).
7. Chen, J. P., Hausladen, M. C., and Yang, R. T., *J. Catal.* **151**, 135 (1995).
8. Yang, R. T., and Li, W. B., *J. Catal.* **155**, 414 (1995).
9. Yang, R. T., and Cichanowicz, J. E., "Pillared Clays as Catalysts for Selective Catalytic Reduction of NO." U.S. Patent 5,415,850 (1995).
10. DelCastillo, H. L., Gil, A., and Grange, P., *Catal. Lett.* **36**, 237 (1996).

11. Yang, R. T., and Baksh, M. S. A., *AIChE J.* **37**, 679 (1991).
12. Cheng, L. S., and Yang, R. T., *Ind. Eng. Chem. Res.* **34**, 2021 (1995).
13. Pinnavaia, T. J., *Science* **220**, 365 (1983).
14. Burch, R., *Catal. Today* **2**, 185 (1988).
15. Figueras, F., *Catal. Rev. Sci. Eng.* **30**, 457 (1988).
16. Czarnecki, L. J., and Anthony, R. G., *AIChE J.* **36**, 794 (1990).
17. Chen, J. P., and Yang, R. T., *J. Catal.* **125**, 411 (1990).
18. He, M. Y., Liu, Z., and Min, E., *Catal. Today* **2**, 321 (1988).
19. Beeckman, J. W., and Hegedus, L. L., *Ind. Eng. Chem. Res.* **30**, 969 (1991).
20. Sterte, J., *Clays and Clay Miner.* **34**, 658 (1986).
21. Sterte, J., "Pillared Clays" (R. Burch, Ed.), *Catal. Today* **2**, 219 (1988).
22. Yamanaka, S., Nishihara, T., Hottori, M., and Suzuki, Y., *Mat. Chem. Phys.* **17** (1987).
23. DelCastillo, H. L., and Grange, P., *Appl. Catal. A*. **103**, 23 (1993).
24. Bernier, A., Admaiai, L. F., and Grange, P., *Appl. Catal.* **77**, 269 (1991).
25. Kato, A., Matsuda, S., Nakajima, F., Imanari, M., and Watanabe, Y., *J. Phys. Chem*. **85**, 1710 (1981).
26. Ackley, M. W., "Separation of Nitrogen and Oxygen by Adsorption." Ph.D. dissertation, SUNY at Buffalo, Buffalo, N.Y., 1991.
27. Tuenter, G., Leeuwen, W. F. V., and Snepvangers, L. J. M., *Ind. Eng. Chem. Prod. Res. Dev.* **25**, 633 (1986).
28. Nabivanets, B. I., and Kudritskaya, L. N., Russ, *J. Inorg. Chem*. **12**, 616 (1969).
29. Grim, R. E., "Clay Mineralogy," p. 56. McGraw-Hill, London, 1953.
30. Baes, C. F., and Mesmer, R. E., "The Hydrolysis of Cations." Wiley, New York, 1976.
31. Einaga, H., *J. Chem. Soc. DaltonTrans.* **1917** (1974).
32. Odenbrand, C. U. I., Andersson, S. L. T., Andersson, L. A. H., Brandin, J. G. M., and Busca, G., *J. Catal.* **125**, 541 (1990).
33. Nobe, K., and Bauerle, G. L., *Ind. Eng. Chem. Prod. Res. Develop.* **14**, 268 (1975).
34. Markvart, M., and Pour, V., *Int. Chem. Eng.* **15**, 546 (1975).
35. Bauerle, G. L., Wu, S. C., and Nobe, K., *Ind. Eng. Chem. Prod. Res. Dev.* **17**, 2 (1978).
36. Curry-Hyde, H. E., and Baiker, A., *Ind. Eng. Chem. Res.* **29**, 1985 (1990).
37. Curry-Hyde, H. E., Musch, H., Baiker, A., Schraml-Marth, M., and Wokaun, A., *J. Catal.* **133**, 397 (1992).
38. Duffy, B. L., Curry-Hyde, H. E., Cant, N. W., and Nelson, P. F., *J. Catal.* **154**, 107 (1995).
39. Schneider, H., Scharf, U., Wokaun, A., and Baiker, A., *J. Catal.* **147**, 545 (1994).
40. Willey, R. J., Lai, H., and Peri, J. B., *J. Catal.* **130**, 319 (1991).
41. Inomata, M., Miyamoto, A., and Murakami, Y., *J. Catal.* **62**, 150 (1980).
42. Van Tol, M. F. H., Quinlan, M. A., Luck, F., Somorjai, G. A., and Nieuwenhuys, B. E., *J. Catal.* **129**, 186 (1991).
43. Topsøe, N.-Y., Slabiak, T., Clausen, B., Srnak, T., and Dumesic, J., *J. Catal.* **134**, 742 (1992).
44. Wong, W. C., and Nobe, K., *Ind. Eng. Chem. Prod. Res. Dev.* **25**, 179 (1986).
45. Morikawa, S., Takahashi, K., Mogi, J., and Kurita, S., *Bull. Chem. Soc. Jpn.* **55**, 2254 (1982).
46. Clark, F. T., Springman, M. C., Willcox, D., and Wachs, I. E., *J. Catal.* **139**, 1 (1993).
47. Murakami, Y., Inomata, M., Mori, K., Ui, T., Suzuki, K., Miyamoto, A., and Hattori, T., *in* "Preparation of Catalysts III" (ed. P. G. Poncelet and P. A. Jacobs, Eds.), p. 531. Elsevier, Amsterdam, 1983.
48. Topsøe, N.-Y., Pedersen, K., and Derouane, E. G., *J. Catal.* **70**, 41 (1981).
49. Odriozola, J. A., Soria, J., Somorjai, G. A., Heinemann, H., Garcia de la Banda, J. F., Granados, M. L., and Conesa, J. C., *J. Phys. Chem*. **95**, 240 (1991).
50. Srnak, T. Z., Demesic, J. A., Clausen, B. S., Törnqvist, E., and Topsøe, N.-Y., *J. Catal.* **135**, 246 (1992).
51. Iizuka, T., Ikeda, H., Terao, T., and Tanabe, K., *Aust. J. Chem*. **35**, 927 (1982).
52. Kung, H. H., "Transition Metal Oxides: Surface Chemistry and Catalysis," Chap. 5. Elsevier, New York (1989).